Data Repository Item 2017080

Schwartz, J.J., Klepeis, K.A., Sadorski, J.F., Stowell, H.H., Tullock, A.J., and Coble, M., 2017, The tempo of continental arc construction in the Mesozoic Median Batholith, Fiordland, New Zealand: Lithosphere, doi:10.1130/L610.1.

DATA REPOSITORY FILE

LIST OF FILES INCLUDED IN DATA REPOSITORY FILE

Data Repository Text: Detailed description of methods.
Data Repository Figure 1: Zircon chondrite normalized rare earth element abundance plots for all samples analyzed in this study.
Data Repository Figure 2: Zircon CL images for all analyzed samples and zircons. Spot locations are indicated with circles. Errors are 1σ.
Data Repository Table 1: U-Pb zircon SHRIMP-RG isotopic data and ages.
Data Repository Table 2: Zircon SHRIMP-RG trace element data.

DATA REPOSITORY TEXT

DETAILED DESCRIPTION OF METHODS

SHRIMP-RG U-Pb zircon geochronology

Data were collected at the USGS-Stanford Ion Microprobe Laboratory at Stanford University, California (Bacon et al, 2012). Five mounts that contained zircons from the 2012 and 2013 field seasons in Fiordland were analyzed during three analytical sessions, from April 1st – 6th, 2012, September 7th – 8th, 2012, and May 23rd – 25th, 2013. Zircon geochronology standard R33 (419 Ma quartz diorite zircon; Black et al., 2004) was added to all five mounts. MADDER, a Stanford University in-house compositional standard was added to mounts 12CSUN4, 13CSUN18B and 13CSUN19. The zircons were aligned in 1 x 6 mm rows on double-sided tape that was placed on glass slides and then cast in a 25 mm diameter by 4mm thick epoxy disc. Mounts were ground and polished to a 1 µm finish, washed with a 1 N HCl solution and thoroughly rinsed in distilled water, and dried in a vacuum oven. Cathodoluminescence Images (CL) were collected using a FEI Quanta 600 Scanning Electron Microscope (SEM) at the California State University scanning electron microscope lab for the purpose of detecting internal structures, inclusions, and physical defects of the zircons. Mounts were coated with ~100Å Au layer and were inspected to ensure uniformity and conductivity before loading into the pre-load instrument chamber. The mounts were stored at high pressure (10-7 torr) for several hours before being moved into the source chamber of the SHRIMP-RG to minimize degassing of the epoxy and isobaric hydride interferences and masses 204-208.

Analyses were performed on the SHRIMP-RG ion microprobe at the USGS-Stanford laboratory utilizing an O_2^- primary ion beam, varying in intensity from 4.3 to 6.4 nA, which produces secondary ions from the target that were accelerated at 10 kV. The analytical spot diameter was between ~15-20 microns and a depth of ~1-2 microns for each analysis performed in this study. Prior to every analysis, the sample surface was cleaned by rastering the primary beam for 60-120 seconds, and the primary and secondary beams were auto-tuned to maximize transmission. The duration of this procedure typically required 2.5 minutes prior to data collection. The acquisition routine for 12CSUN1, 12CSUN4, and 12CSUN5 included $^{89}Y^+$, 9-REE ($^{139}La^+$, $^{140}Ce^+$, $^{146}Nd^+$, $^{147}Sm^+$, $^{153}Eu^+$, $^{155}Gd^+$, $^{163}Dy^{16}O^+$, $^{166}Er^{16}O^+$, $^{172}Yb^{16}O^+$), a high mass normalizing species ($^{90}Zr_2{}^{16}O^+$), followed by $^{180}Hf^{16}O^+$, $^{204}Pb^+$, a background measured at 0.045 mass units above the $^{204}Pb^+$ peak, $^{206}Pb^+$, $^{207}Pb^+$, $^{208}Pb^+$, $^{232}Th^+$, $^{238}U^+$, $^{232}Th^{16}O^+$, and $^{238}U^{16}O^+$. Measurements were made at mass resolutions of $M/\Delta M$ = 8100-8400 (10% peak height), which eliminated interfering molecular species, particularly for the REE. For mounts 13CSUN18B and 13CSUN19, the analysis routine was the same as above, but also included masses $^{30}Si^{16}O^+$, $^{48}Ti^+$, $^{49}Ti^+$, and $^{56}Fe^+$. Measurements for these mounts were performed at a mass resolutions of $M/\Delta M$ = 9000-9500, which was required to fully separate the $^{48}Ti^+$ peak from the nearby $^{96}Zr^{++}$ peak. Analyses consisted of 5 peak-hopping cycles stepped sequentially through the run table. The duration of each measurement ranged between 15-25 minutes on average. Count times for most elements was between 1-8 seconds, with increased count times ranging from 15-30 seconds for ^{204}Pb, ^{206}Pb, ^{207}Pb, and ^{208}Pb to improve counting statistics and age precision. Similar to previous studies, U concentrations were quite low (roughly <200 ppm) for zircons from mafic to intermediate composition rocks. R33 was analyzed after every 3-5 unknown zircons. Average count rates of each element were ratioed to the appropriate high mass normalizing species to account for any primary current drift, and the derived ratios for the unknowns were compared to an average of those for the standards to determine concentrations.

Spot-to-spot precisions (as measured on the standards) varied according to elemental ionization efficiency and concentration.

Data reduction for geochronologic results followed the methods described by Williams (1997), and Ireland & Williams (2003), and used the MS Excel add-in programs Squid 2.51 and Isoplot 3.76 of Ken Ludwig (2009; 2012). The data produced from mounts 12CSUN1, 12CSUN4, and 12CSUN5 were initially reduced using Squid 1.13 and Isoplot 3; however during the third analytical session, the 2012 data were processed using newer Squid 2.51 reduction parameters for consistency. Mounts 13CSUN18B and 13CSUN19 were also processed using Squid 2.51. The measured $^{206}Pb/^{238}U$ was corrected for common Pb using ^{207}Pb, whereas $^{207}Pb/^{206}Pb$ was corrected using ^{204}Pb following methods by Tera and Wasserburg (1972) and Stacey and Kramers (1975). The common Pb correction was based on a model Pb composition from Stacey and Kramers (1975). No addition error was propagated for the uncertainty in the common Pb composition. All reported $^{206}Pb/^{238}U$ and $^{207}Pb/^{206}Pb$ model ages and uncertainties (2σ) include error summed in quadrature from the external reproducibility (1σ SD) of the standard R33 during an individual analytical session (16-24 hours). The 1σ standard error of the mean for the reproducibility of the standard was also propagated into the final calculated $^{206}Pb/^{238}U$ weighted mean age.

Weighted average and Tera Wasserburg Concordia intercept ages were calculated using SQUID2 processed data in Isoplot 3 add-on for Microsoft Excel (Tera & Wasserburg, 1972). The Concordia and weighted average plots that express the crystallization ages for the samples used MSWD to distinguish overdispersion within a sample. MSWD is defined as:

$$\mathrm{MSWD} = f^{-1}\, \Sigma(\Delta y_i^2 / \sigma_i^2)$$

Where $f = (n\text{-}2)$ degrees of freedom, and n represents the total number of data points, $\Delta y_i = y_i - ax_i - b$, is the deviation of the ith point and $\sigma_i^2 = \sigma^2(\Delta y) = a^2\sigma_{xi}^2 + \sigma_{yi}^2$, is the square of the error. An MSWD close to or equal to 1 occurs if the assigned error is the only cause of the scatter. A value greatly exceeding an MSWD of 1 is due to either: 1) non-analytical errors, such as a geologic phenomenon that creates the deviation from the mean, or 2) an underestimation of the assigned error. MSWD values that are less than one are a product of possible overestimation of the analytical error or an unrecognized error correlation.

Trace Element Methods

For the zircon standards MAD-green (4196 ppm U, Barth and Wooden, 2010) and MADDER (3435 ppm U), precision generally ranged from about ±3% for Hf, ±5-10% for the Y and HREE, ±10-15%, and up to ±40% for La which was present most often at the ppb level (all values at 2σ).Trace elements (Y, Hf, REE) were measured briefly (typically 1 to 3 sec/mass) immediately before the geochronology peaks in mass order. All peaks were measured on a single EPT® discrete-dynode electron multiplier operated in pulse counting mode. Analyses were performed using 5 scans (peak-hopping cycles from mass 46 through 254), and counting times on each peak were varied according to the sample age as well as the U and Th concentrations in order to improve counting statistics and age precision.

For mounts 12CSUN1, 12CSUN4, and 12CSUN5 zircon concentrations for U, Th and all of the measured trace elements were standardized against a well-characterized, homogeneous zircon standard, MAD-green (Barth and Wooden, 2010), which was mounted on a separate setup mount. U, Th, and trace element concentrations for mounts 13CSUN18b and 13CSUN19 were calculated relative to MADDER, which is calibrated relative to MAD-green. Chondrite normalized plots were calculated using values from McDonough & Sun (1995).

REFERENCES

Aleinikoff, J.N., Wintsch, R.P., Tollo, R.P., Unruh, D.M., Fanning, C.M., and Schmitz, M.D., 2007, Ages and origins of rocks of the Killingworth Dome, south-central Connecticut: implications for the tectonic evolution of southern New England, American Journal of Science, v. 307, p. 63-118.

Barth, A. P., and Wooden, J.L., 2010, Coupled elemental and isotopic analyses of polygenetic zircons from granitic rocks by ion microprobe, with implications for melt evolution and the source of granitic magmas. Chemical Geology, 277, p. 149-159.

Black, L.P., Kamo, S.L., Allen, C.M., Davis, D.W., Aleinikoff, J.N., Valley, J.W., Mundil, R., Campbell, I.H., Korsch, R.J., Williams, I.S., and Foudoulis, C., 2004, Improved $^{206}Pb/^{238}U$ microprobe geochronology by the monitoring of a trace-element-related matrix effect; SHRIMP, ID–TIMS, ELA–ICP–MS and oxygen isotope documentation for a series of zircon standards, Chemical Geology, v. 205, p. 115-140.

Clement, S.W.J., and Compston, W., 1994, Ion probe parameters for very high resolution without loss of sensitivity. U.S. Geological Survey Circ. 1107, p. 62.

Ireland, T.R., and Williams, I.S., 2003, considerations in zircon geochronology by SIMS, Reviews in Mineralogy and Geochemistry, v. 53, p. 215-241, Hanchar, J.M. and Hoskin, W.O., editors.

Ludwig, K.R., 2009, Squid 2, A user’s manual, Berkeley Geochronology Center Special Publication No. 5, p. 110.

Ludwig, K.R., 2012, Isoplot 3.75, a geochronological toolkit for Excel, Berkeley Geochronology Center Special Publication No. 5, p. 75.

Mazdab, F.K., 2009, Characterization of flux-grown trace-element-doped titanite using the high-mass-resolution ion microprobe (SHRIMP-RG), The Canadian Mineralogist, v. 47, p. 813-831.

Sparks, M.A., Needy, S.K., Roell, J.L., Carter, C.A., Geyer, M., Barth, A.P., Wooden, J.L., and Mazdab, F., 2008, Geologic history of a gneissic suite from southeastern California: GSA Abstracts with Programs 40, no. 5, p. 28.

Stacey, J. and Kramers, J.D. 1975, Approximation of terrestrial lead isotope evolution by a two-stage model: Earth and Planetary Science Letters, 26, 207–221.

Williams, I.S., 1997, U-Th-Pb geochronology by ion microprobe: not just ages but histories. Society Economic Geologists Rev. Econ. Geol., v. 7, p. 1-35.

Data Repository Figure 1

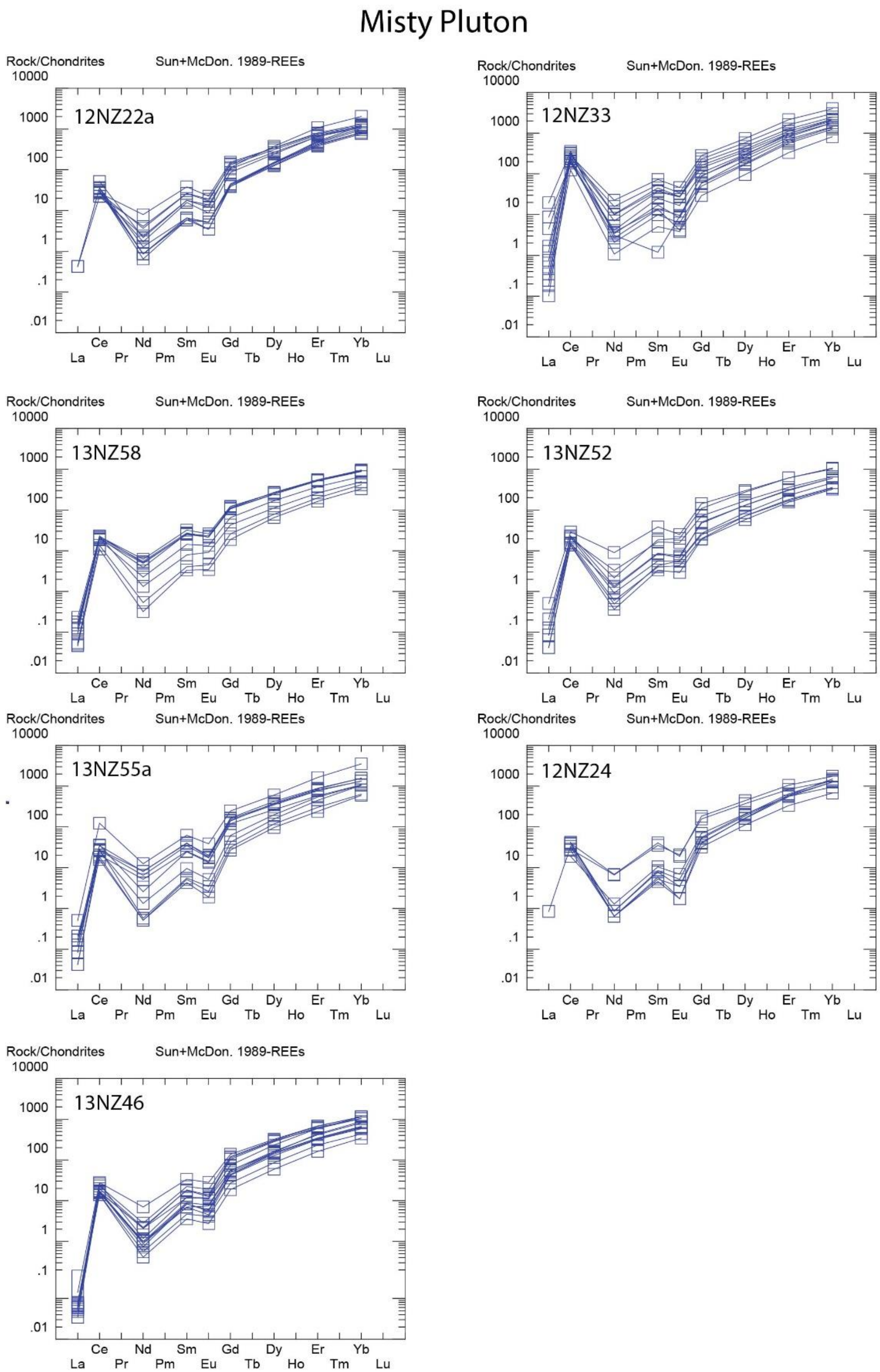

Malaspina Pluton

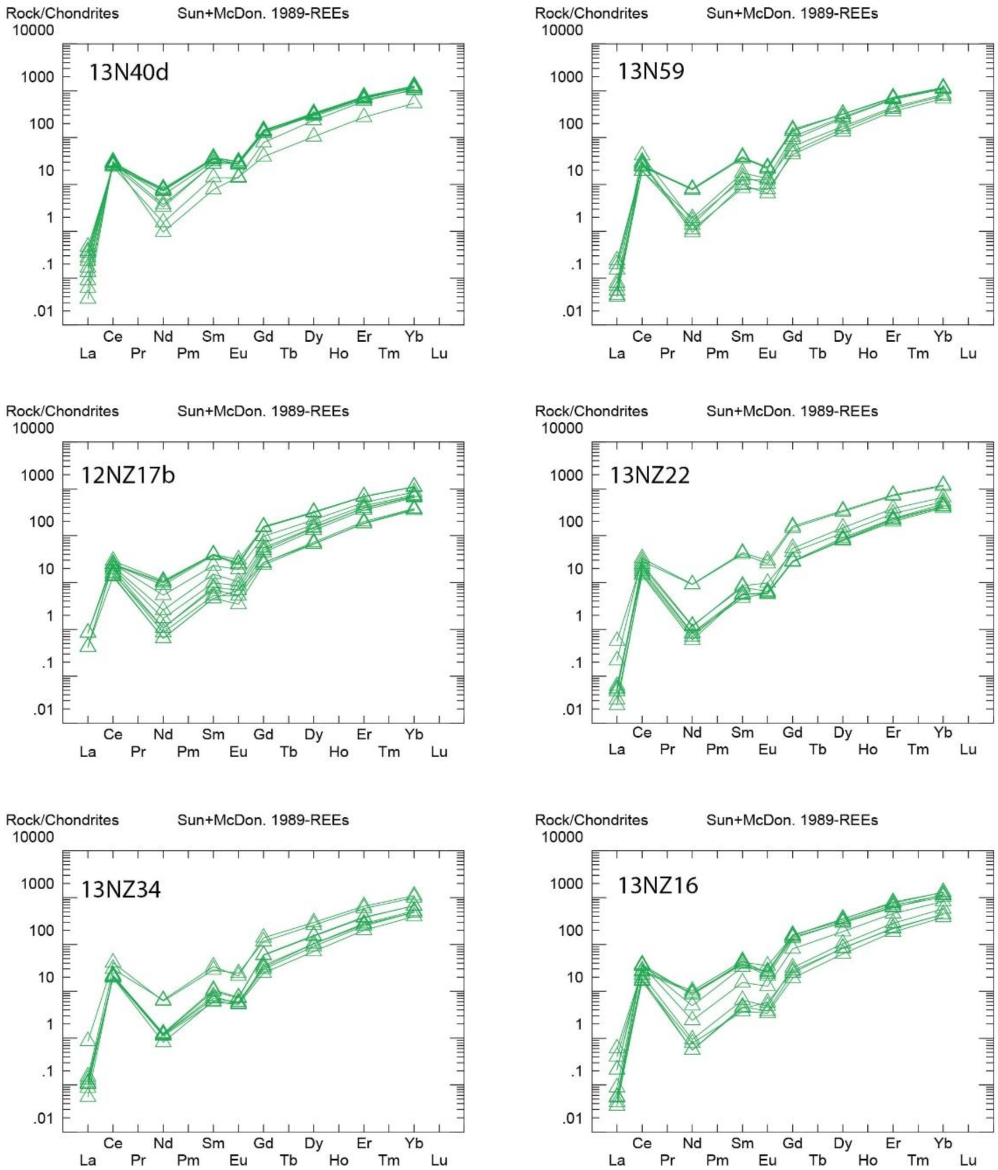

149

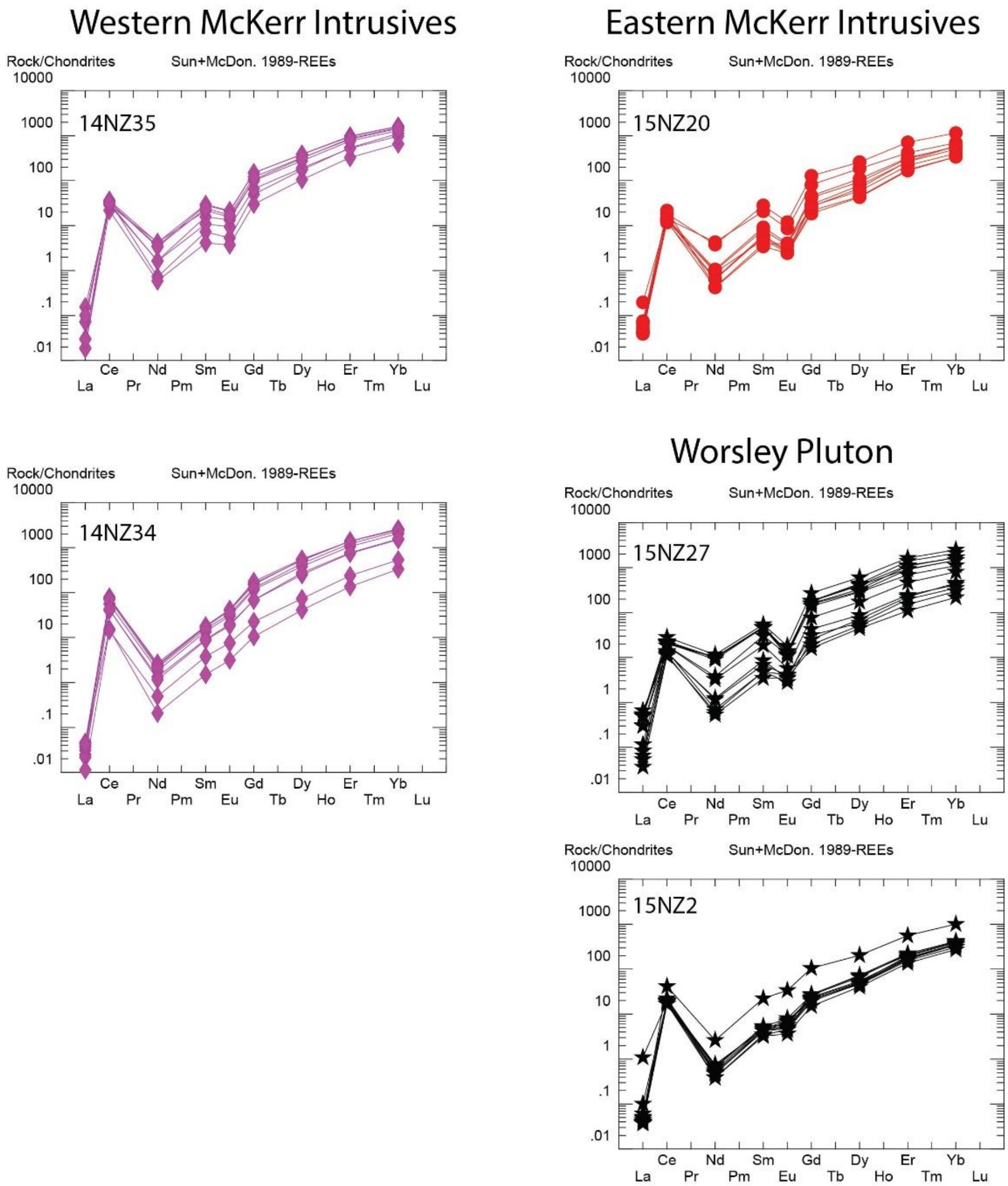
Western McKerr Intrusives
Eastern McKerr Intrusives
Worsley Pluton
Rock/Chondrites
Sun+McDon. 1989-REEs
14NZ35
14NZ34
15NZ20
15NZ27
15NZ2
10000
1000
100
10
1
.1
.01
La Ce Pr Nd Pm Sm Eu Gd Tb Dy Ho Er Tm Yb Lu

Data Repository Figure 2

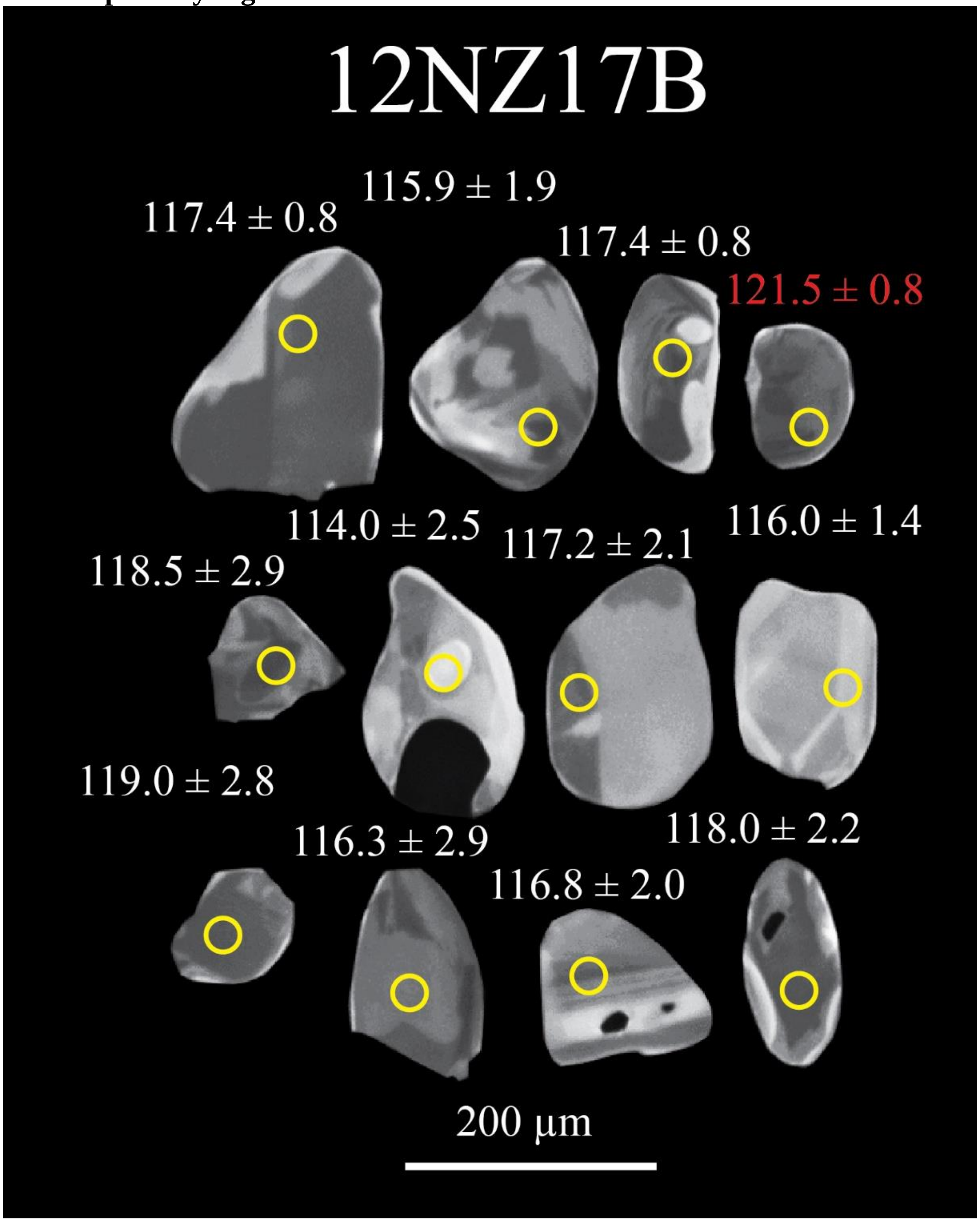

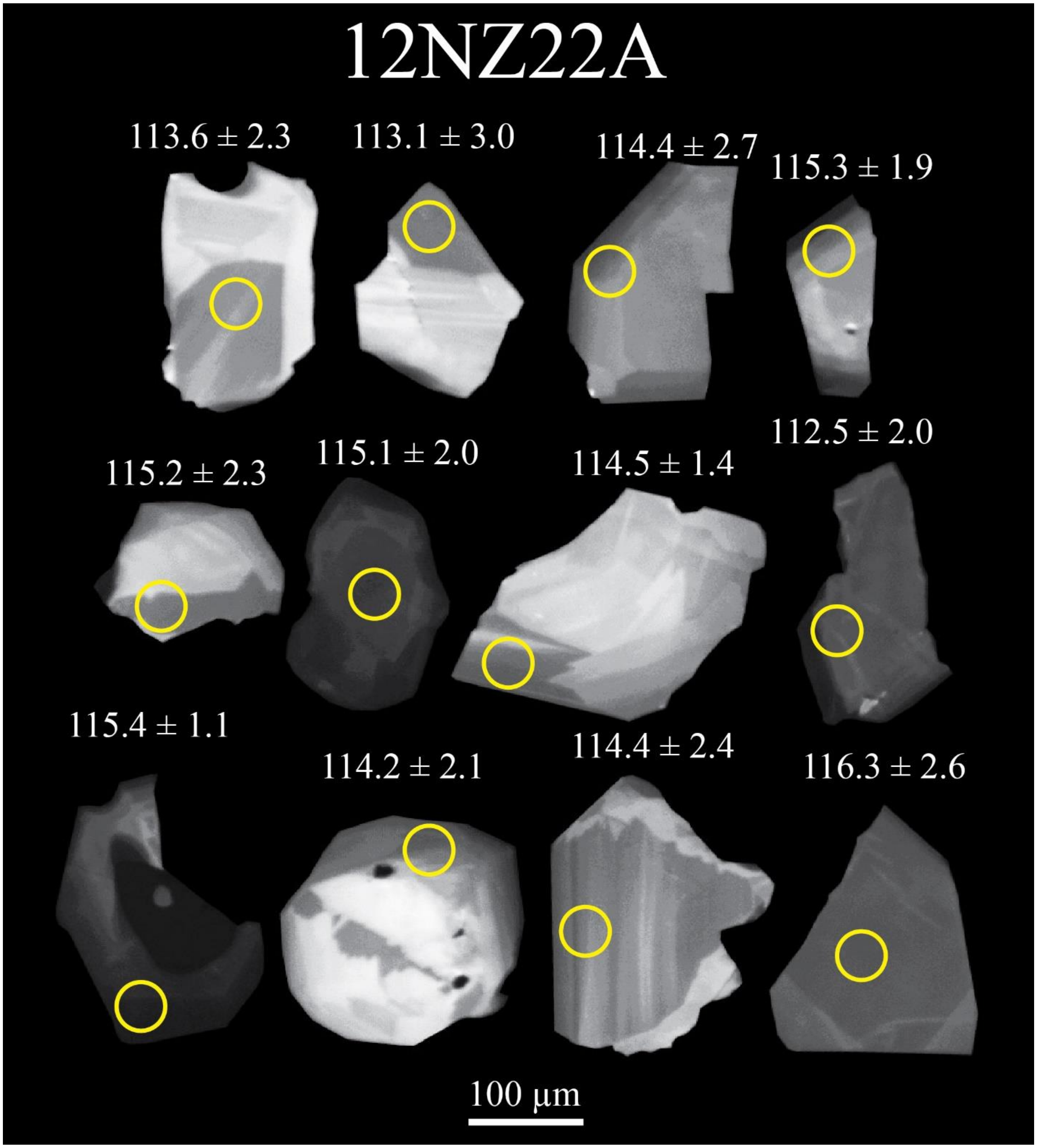
12NZ22A
113.6 ± 2.3
113.1 ± 3.0
114.4 ± 2.7
115.3 ± 1.9
115.2 ± 2.3
115.1 ± 2.0
114.5 ± 1.4
112.5 ± 2.0
115.4 ± 1.1
114.2 ± 2.1
114.4 ± 2.4
116.3 ± 2.6
100 µm

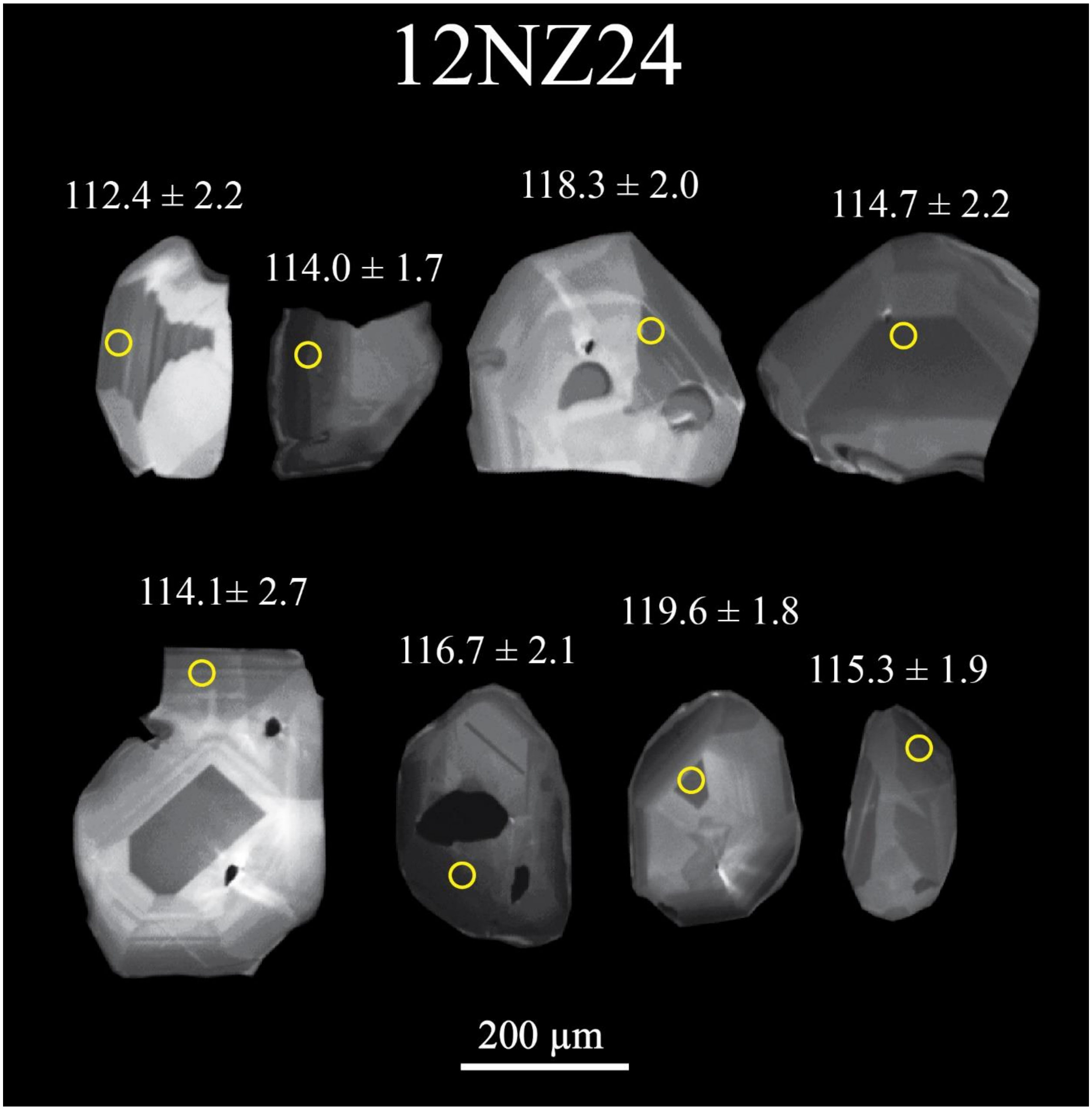
12NZ24
112.4 ± 2.2
114.0 ± 1.7
118.3 ± 2.0
114.7 ± 2.2
114.1± 2.7
116.7 ± 2.1
119.6 ± 1.8
115.3 ± 1.9
200 μm

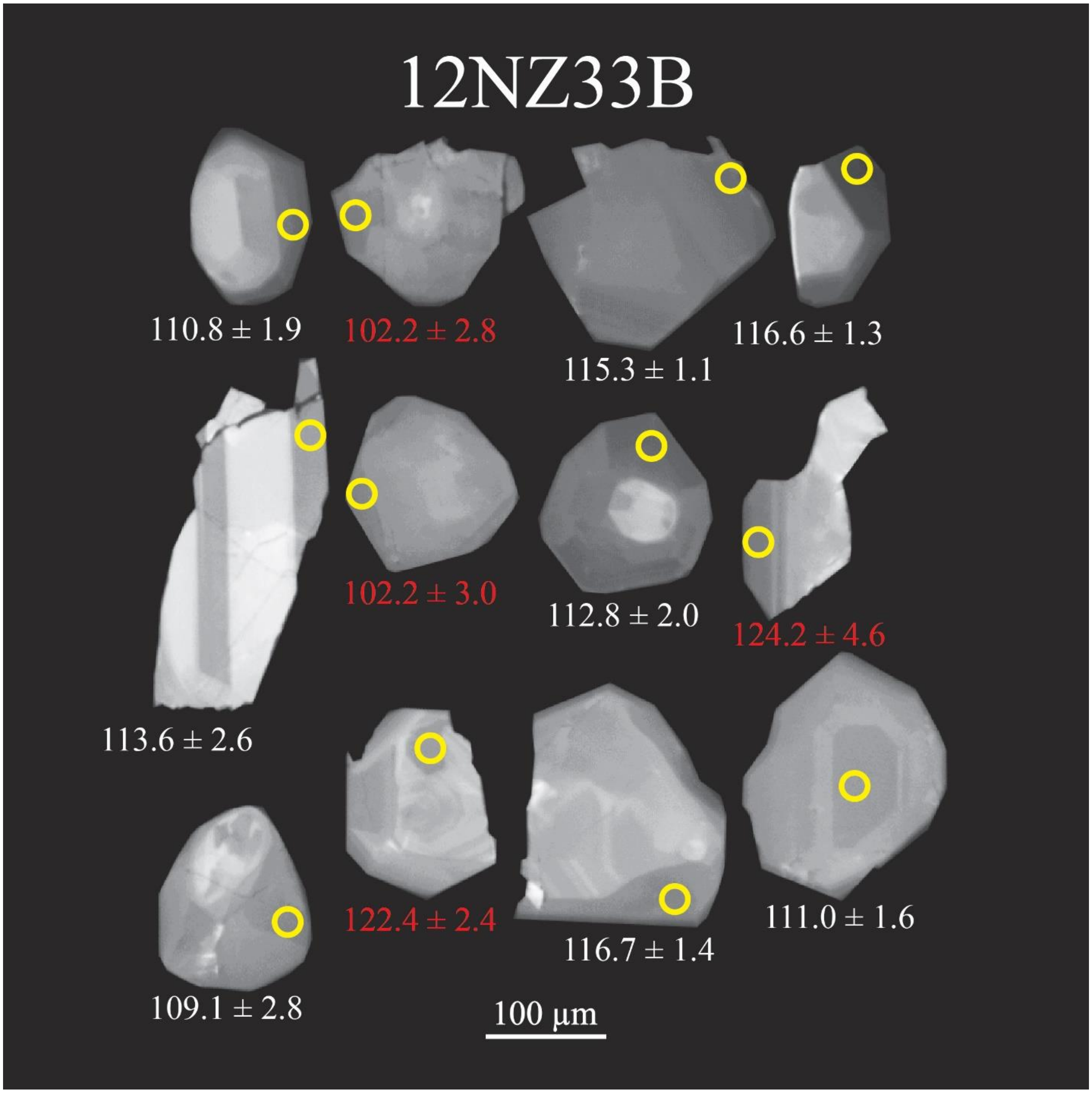
12NZ33B
110.8 ± 1.9
102.2 ± 2.8
115.3 ± 1.1
116.6 ± 1.3
113.6 ± 2.6
102.2 ± 3.0
112.8 ± 2.0
124.2 ± 4.6
109.1 ± 2.8
122.4 ± 2.4
116.7 ± 1.4
111.0 ± 1.6
100 μm

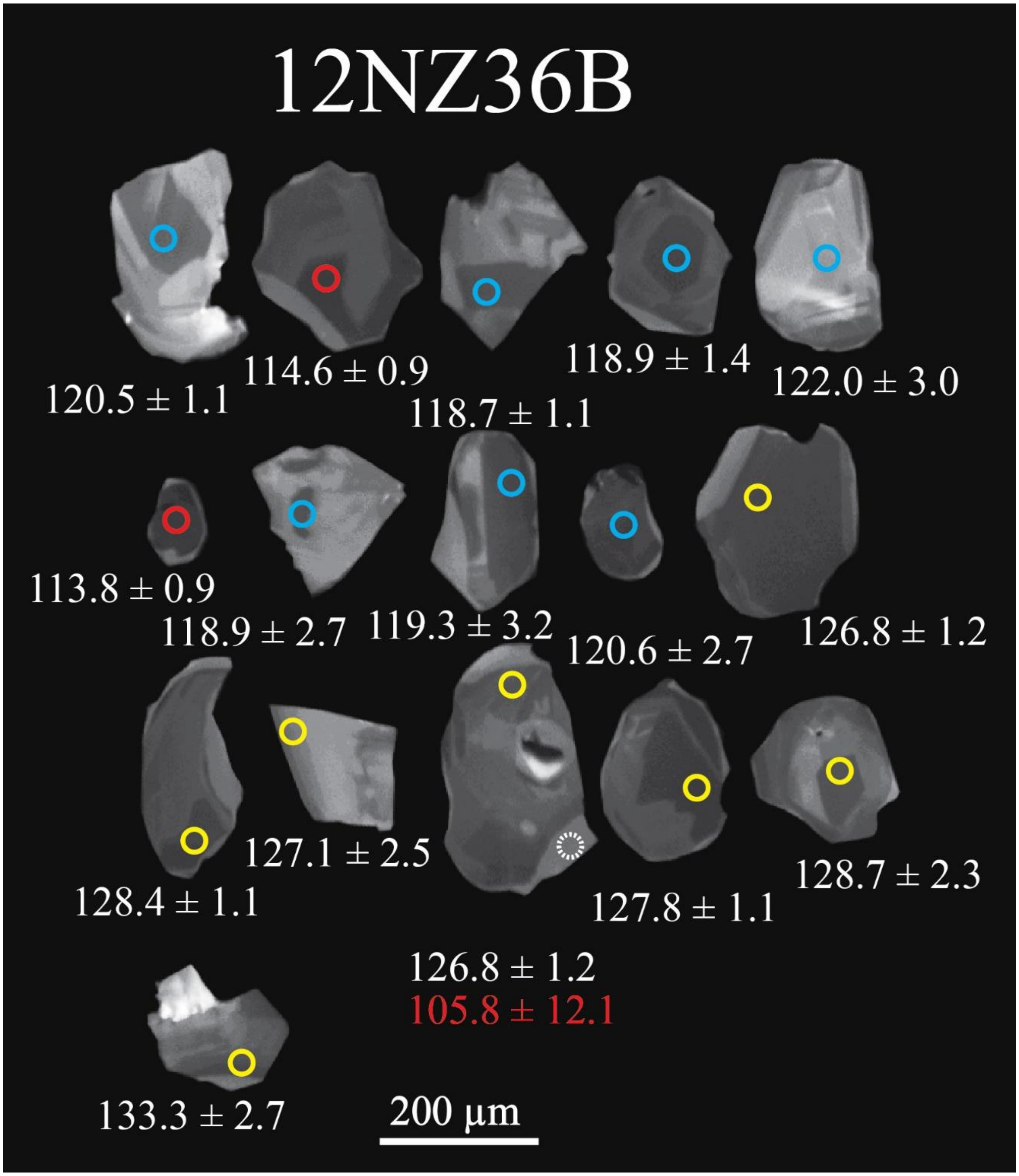
12NZ36B
120.5 ± 1.1
114.6 ± 0.9
118.7 ± 1.1
118.9 ± 1.4
122.0 ± 3.0
113.8 ± 0.9
118.9 ± 2.7
119.3 ± 3.2
120.6 ± 2.7
126.8 ± 1.2
128.4 ± 1.1
127.1 ± 2.5
127.8 ± 1.1
128.7 ± 2.3
126.8 ± 1.2
105.8 ± 12.1
133.3 ± 2.7
200 µm

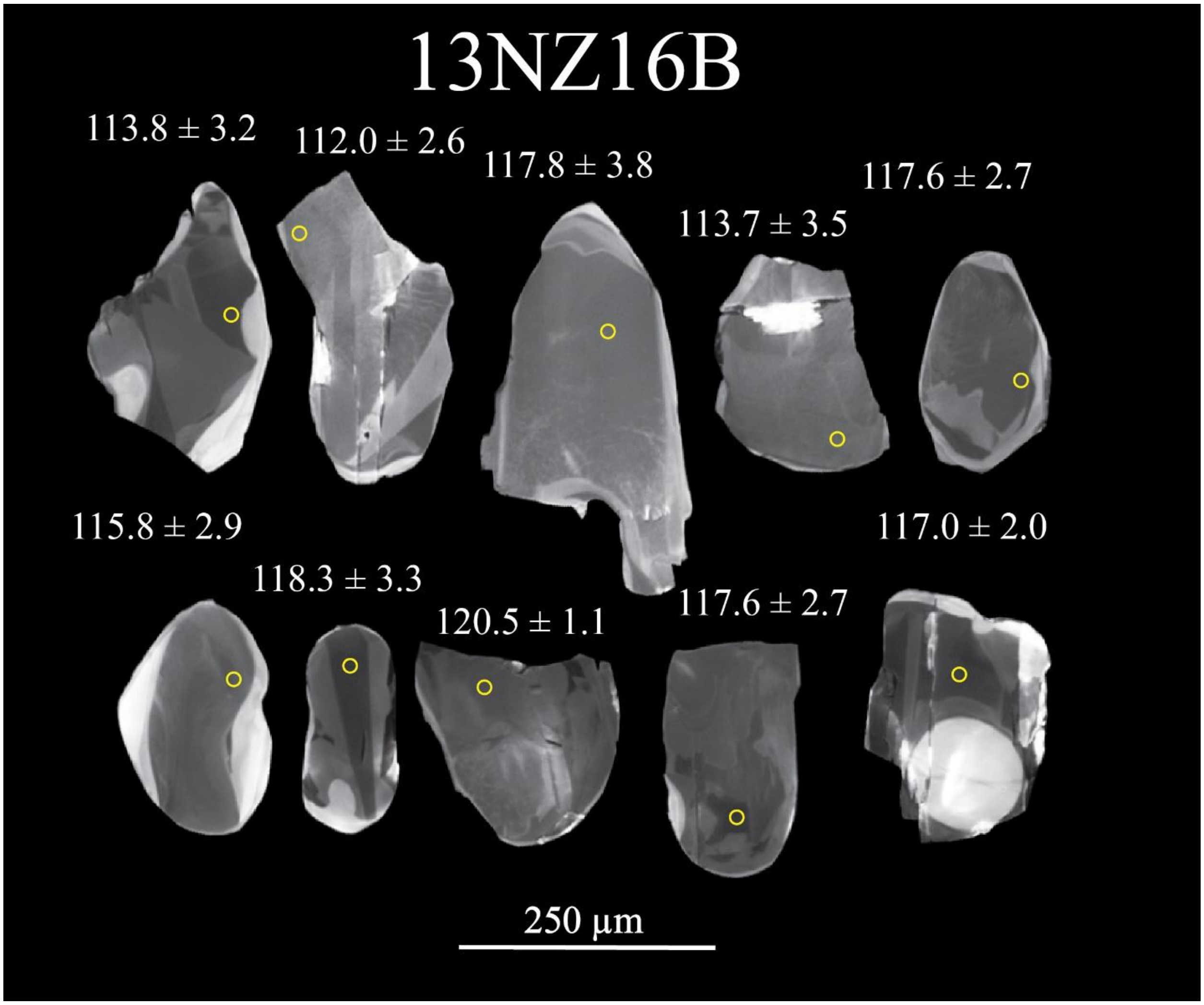
13NZ16B
113.8 ± 3.2
112.0 ± 2.6
117.8 ± 3.8
113.7 ± 3.5
117.6 ± 2.7
115.8 ± 2.9
118.3 ± 3.3
120.5 ± 1.1
117.6 ± 2.7
117.0 ± 2.0
250 μm

159 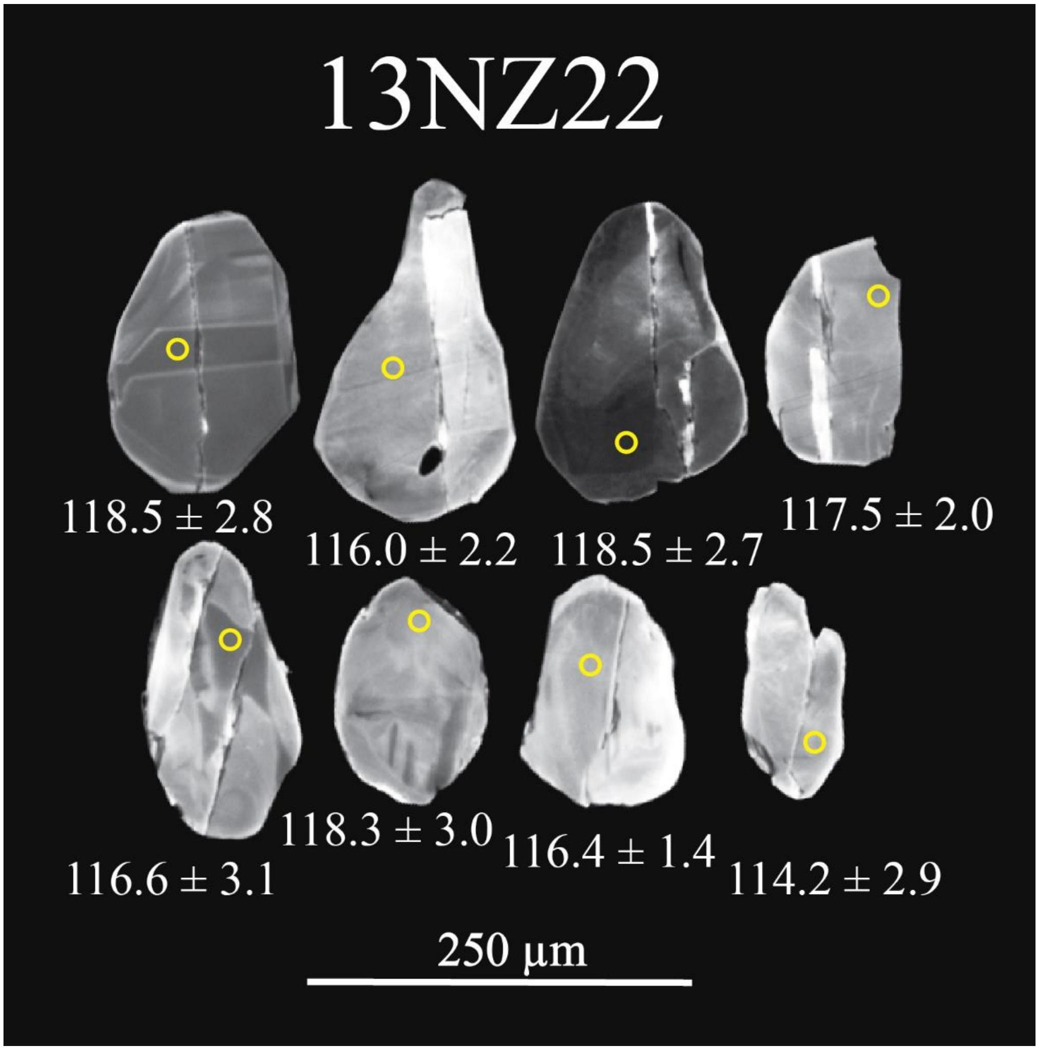
13NZ22
118.5 ± 2.8
116.0 ± 2.2
118.5 ± 2.7
117.5 ± 2.0
116.6 ± 3.1
118.3 ± 3.0
116.4 ± 1.4
114.2 ± 2.9
250 µm

160 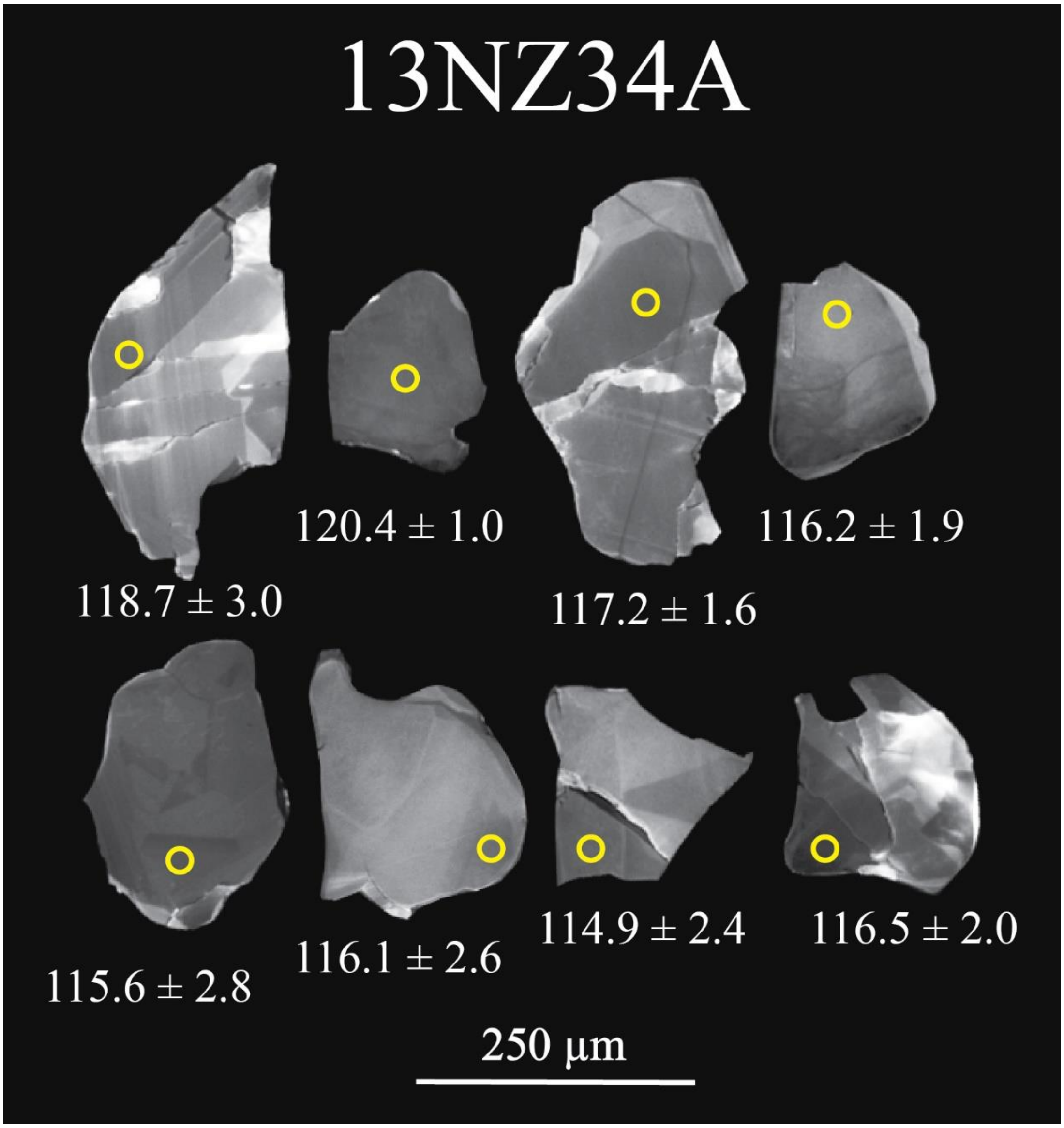
13NZ34A
118.7 ± 3.0
120.4 ± 1.0
117.2 ± 1.6
116.2 ± 1.9
115.6 ± 2.8
116.1 ± 2.6
114.9 ± 2.4
116.5 ± 2.0
250 µm

161 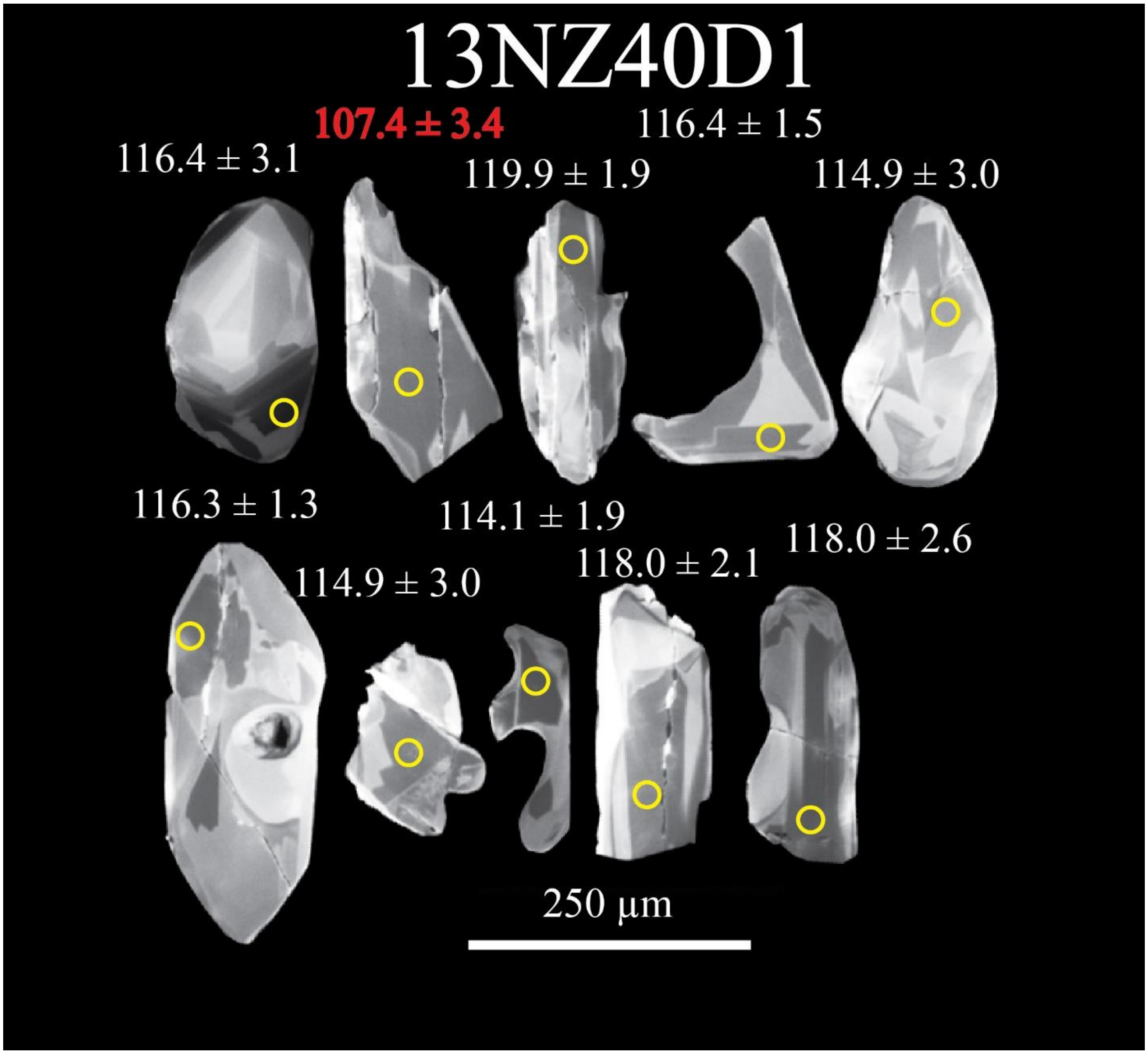
13NZ40D1
107.4 ± 3.4
116.4 ± 1.5
116.4 ± 3.1
119.9 ± 1.9
114.9 ± 3.0
116.3 ± 1.3
114.1 ± 1.9
118.0 ± 2.6
118.0 ± 2.1
114.9 ± 3.0
250 μm

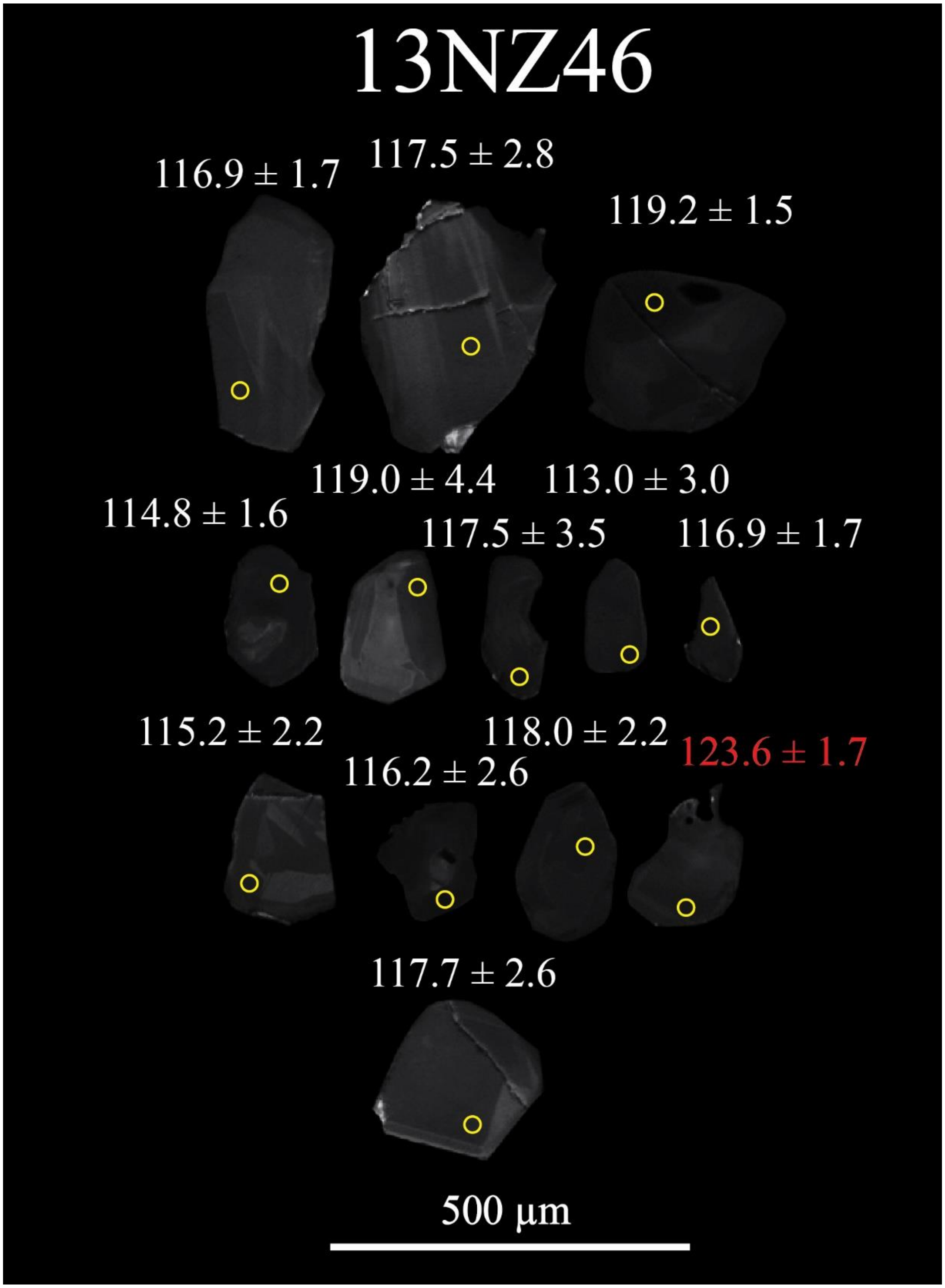
13NZ46
116.9 ± 1.7
117.5 ± 2.8
119.2 ± 1.5
119.0 ± 4.4
113.0 ± 3.0
114.8 ± 1.6
117.5 ± 3.5
116.9 ± 1.7
115.2 ± 2.2
118.0 ± 2.2
123.6 ± 1.7
116.2 ± 2.6
117.7 ± 2.6
500 μm

162

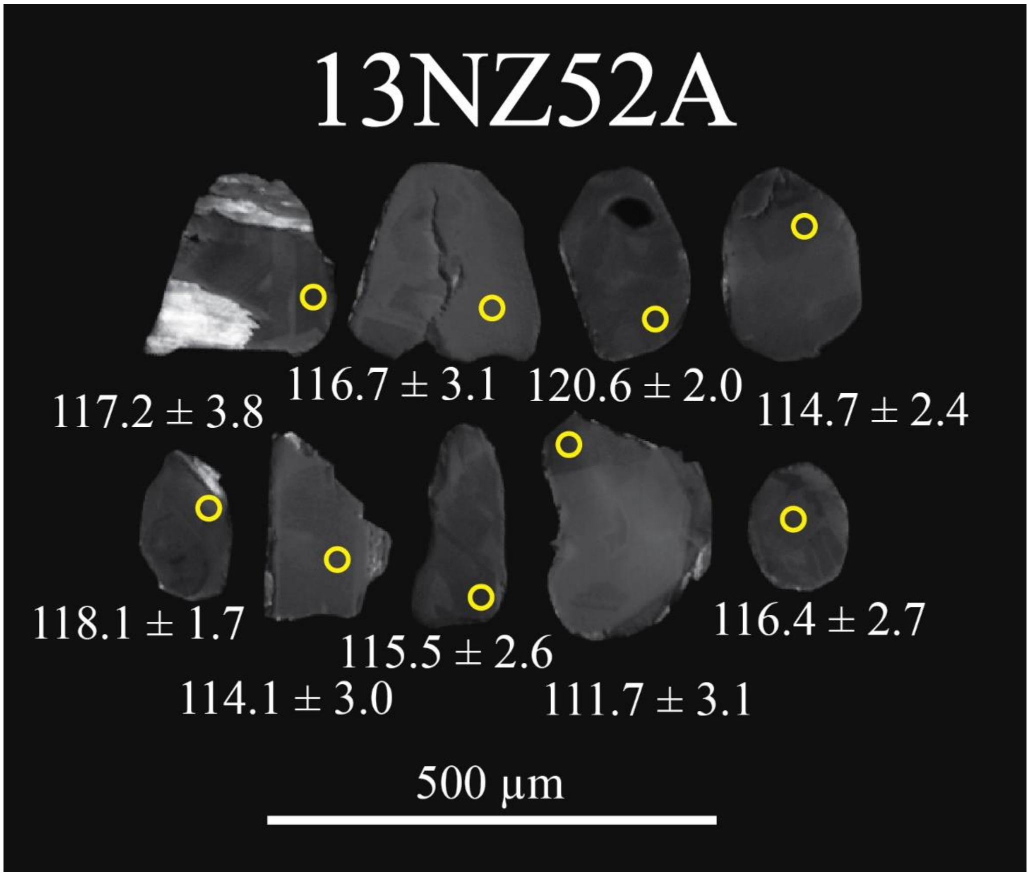
13NZ52A
117.2 ± 3.8
116.7 ± 3.1
120.6 ± 2.0
114.7 ± 2.4
118.1 ± 1.7
114.1 ± 3.0
115.5 ± 2.6
111.7 ± 3.1
116.4 ± 2.7
500 µm

164 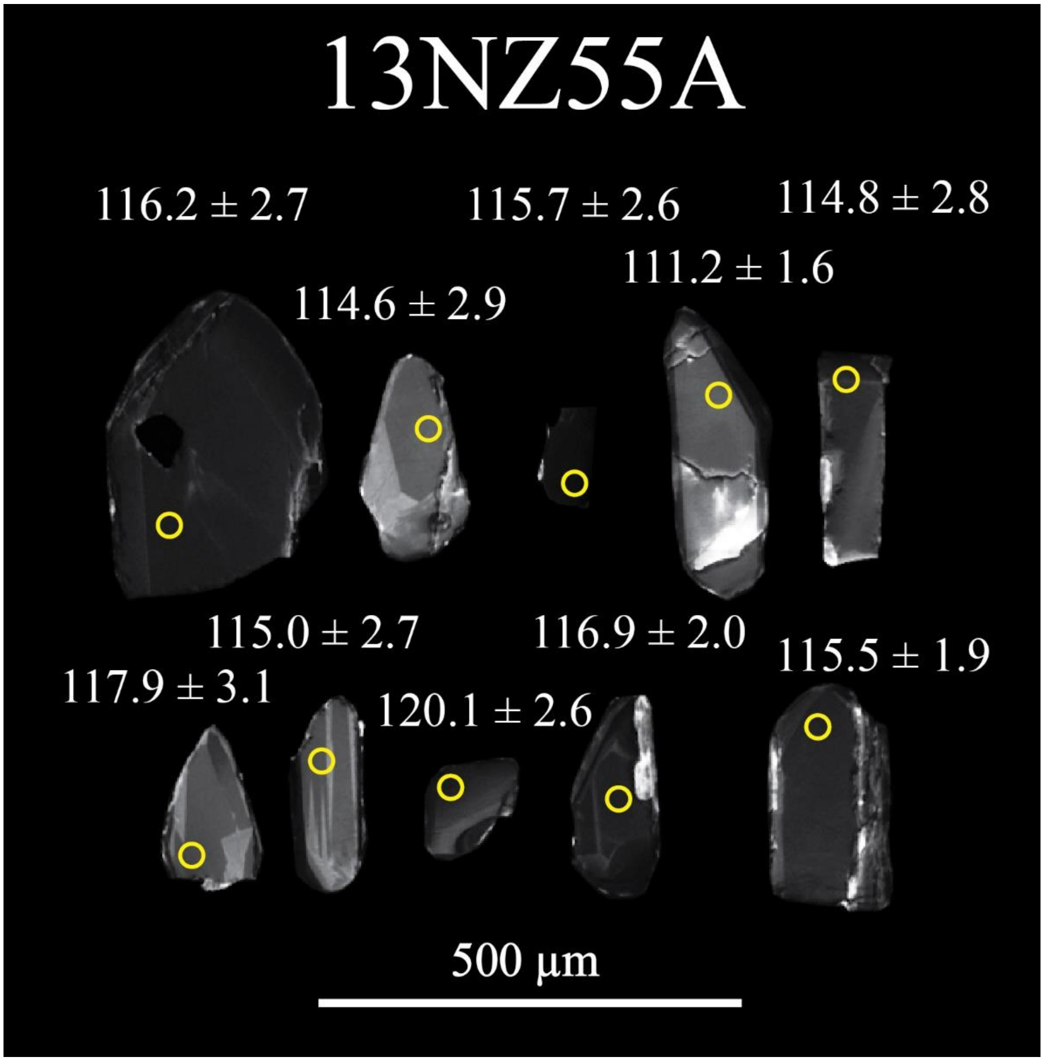
13NZ55A
116.2 ± 2.7
115.7 ± 2.6
114.8 ± 2.8
111.2 ± 1.6
114.6 ± 2.9
115.0 ± 2.7
116.9 ± 2.0
115.5 ± 1.9
117.9 ± 3.1
120.1 ± 2.6
500 µm

165 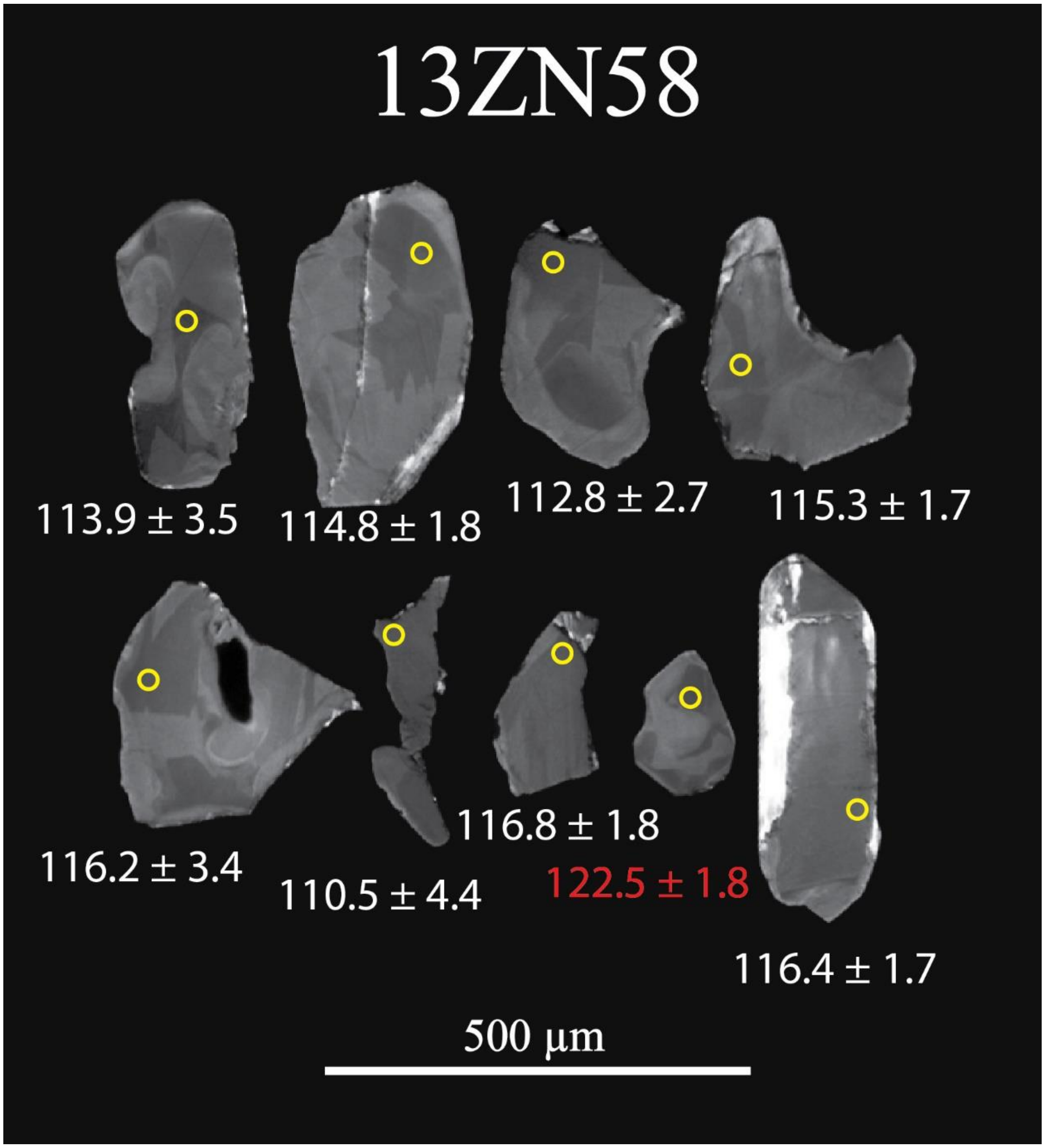
13ZN58
113.9 ± 3.5
114.8 ± 1.8
112.8 ± 2.7
115.3 ± 1.7
116.2 ± 3.4
110.5 ± 4.4
116.8 ± 1.8
122.5 ± 1.8
116.4 ± 1.7
500 µm

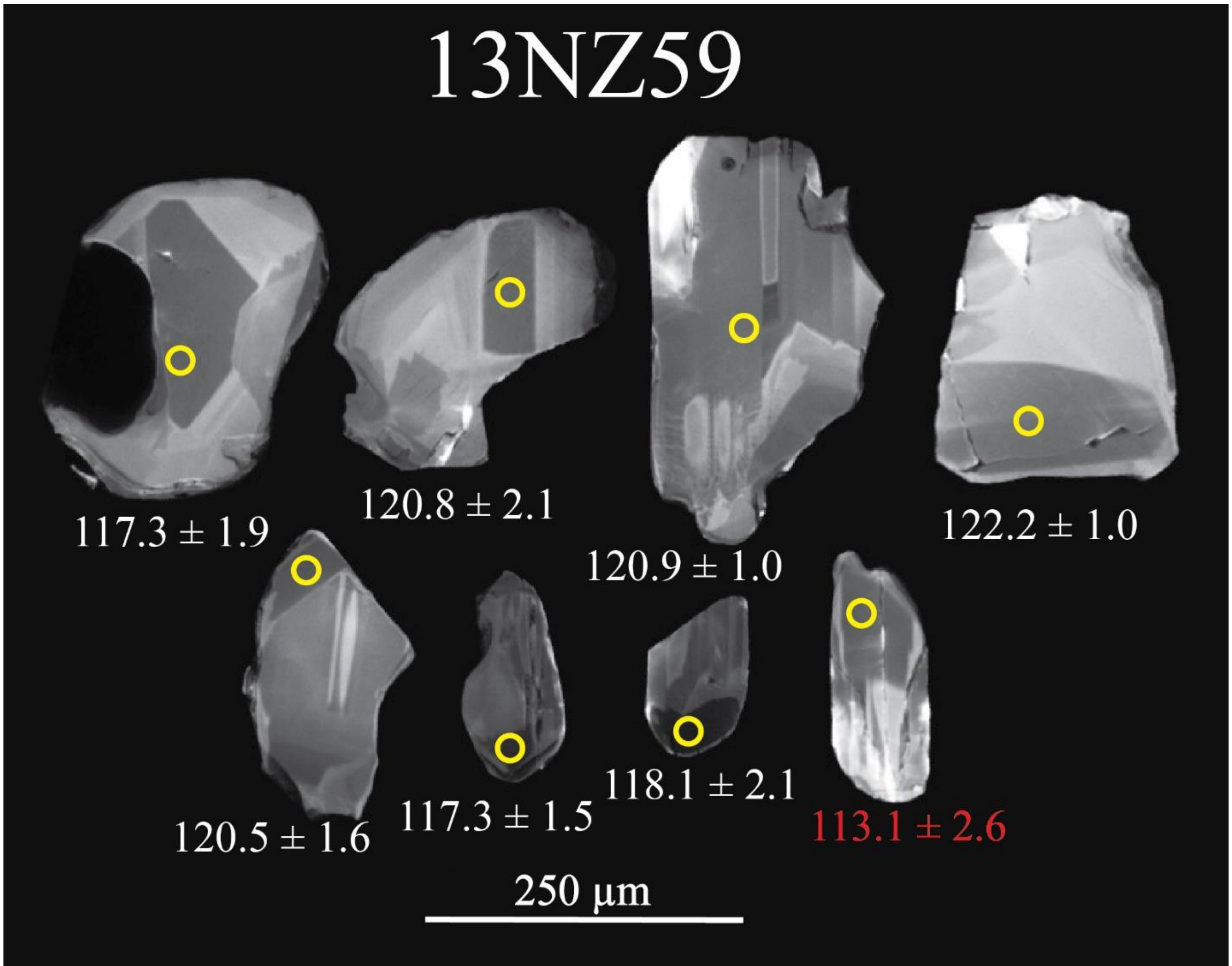
13NZ59
117.3 ± 1.9
120.8 ± 2.1
120.9 ± 1.0
122.2 ± 1.0
120.5 ± 1.6
117.3 ± 1.5
118.1 ± 2.1
113.1 ± 2.6
250 µm

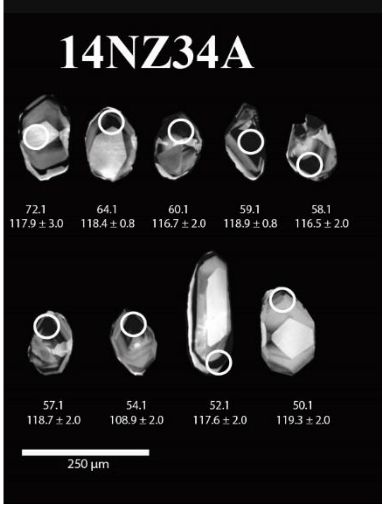
14NZ34A
72.1
117.9 ± 3.0
64.1
118.4 ± 0.8
60.1
116.7 ± 2.0
59.1
118.9 ± 0.8
58.1
116.5 ± 2.0
57.1
118.7 ± 2.0
54.1
108.9 ± 2.0
52.1
117.6 ± 2.0
50.1
119.3 ± 2.0
250 µm

168 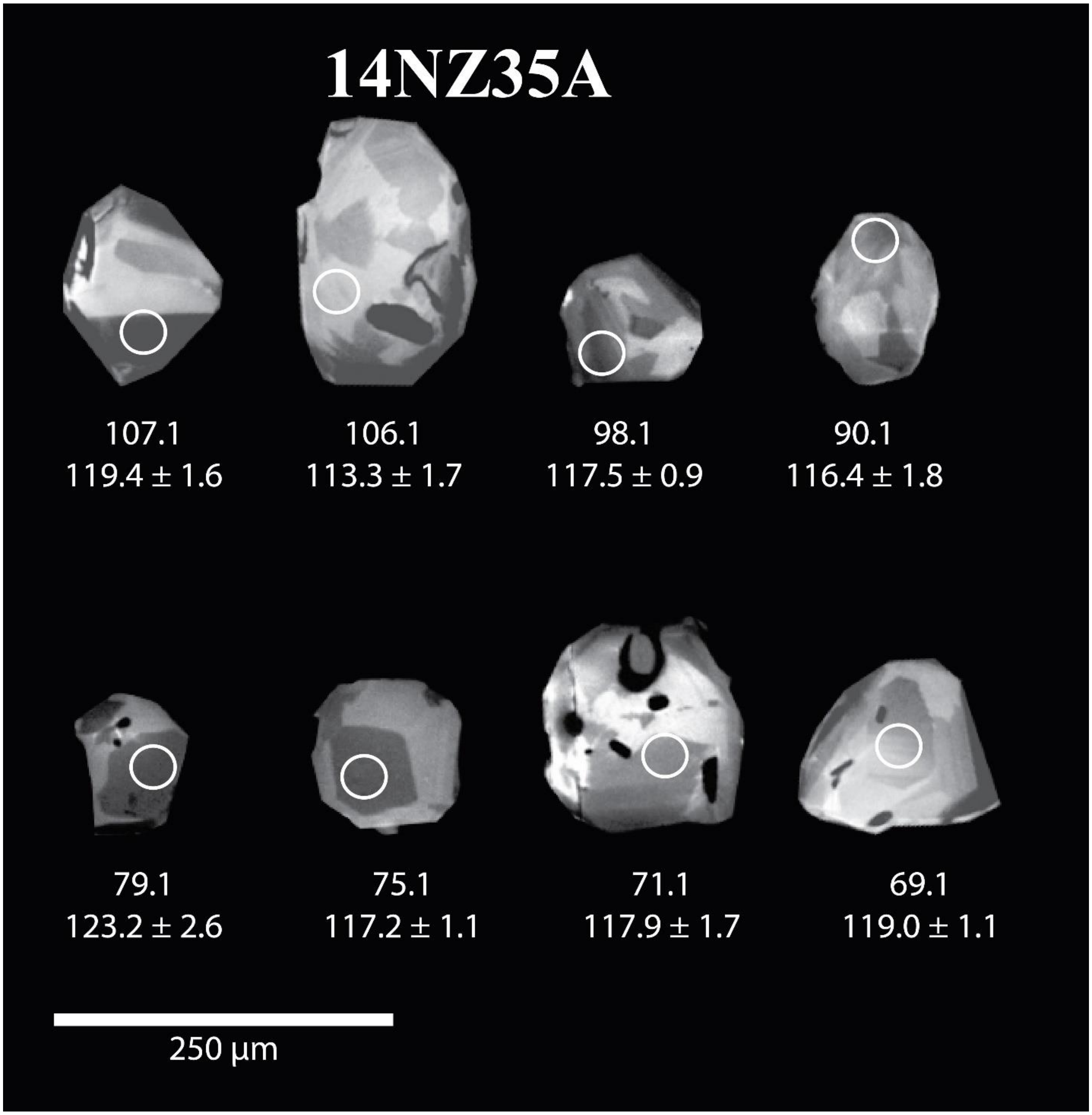
14NZ35A
107.1
119.4 ± 1.6
106.1
113.3 ± 1.7
98.1
117.5 ± 0.9
90.1
116.4 ± 1.8
79.1
123.2 ± 2.6
75.1
117.2 ± 1.1
71.1
117.9 ± 1.7
69.1
119.0 ± 1.1
250 µm

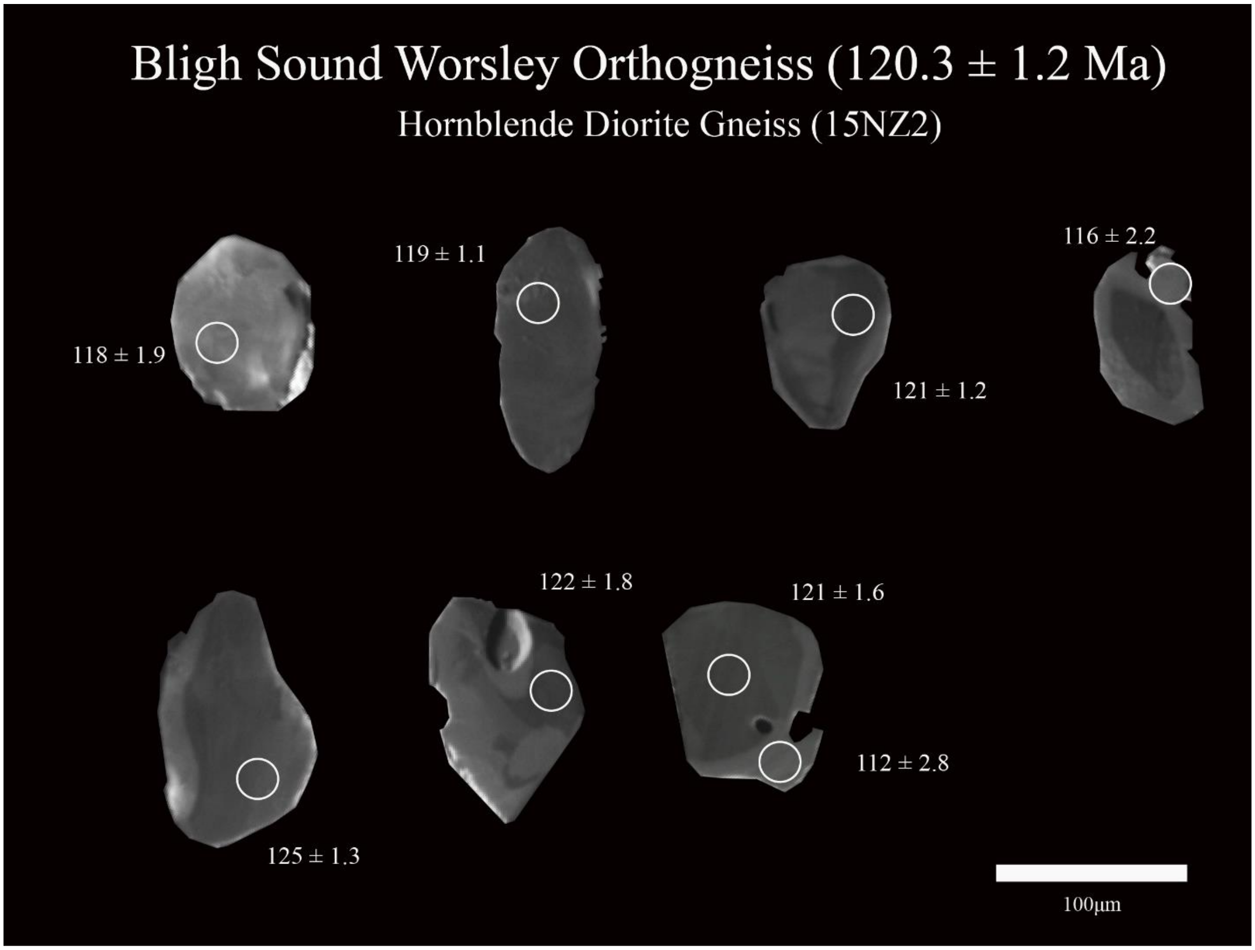
Bligh Sound Worsley Orthogneiss (120.3 ± 1.2 Ma)
Hornblende Diorite Gneiss (15NZ2)
118 ± 1.9
119 ± 1.1
121 ± 1.2
116 ± 2.2
122 ± 1.8
121 ± 1.6
112 ± 2.8
125 ± 1.3
100μm

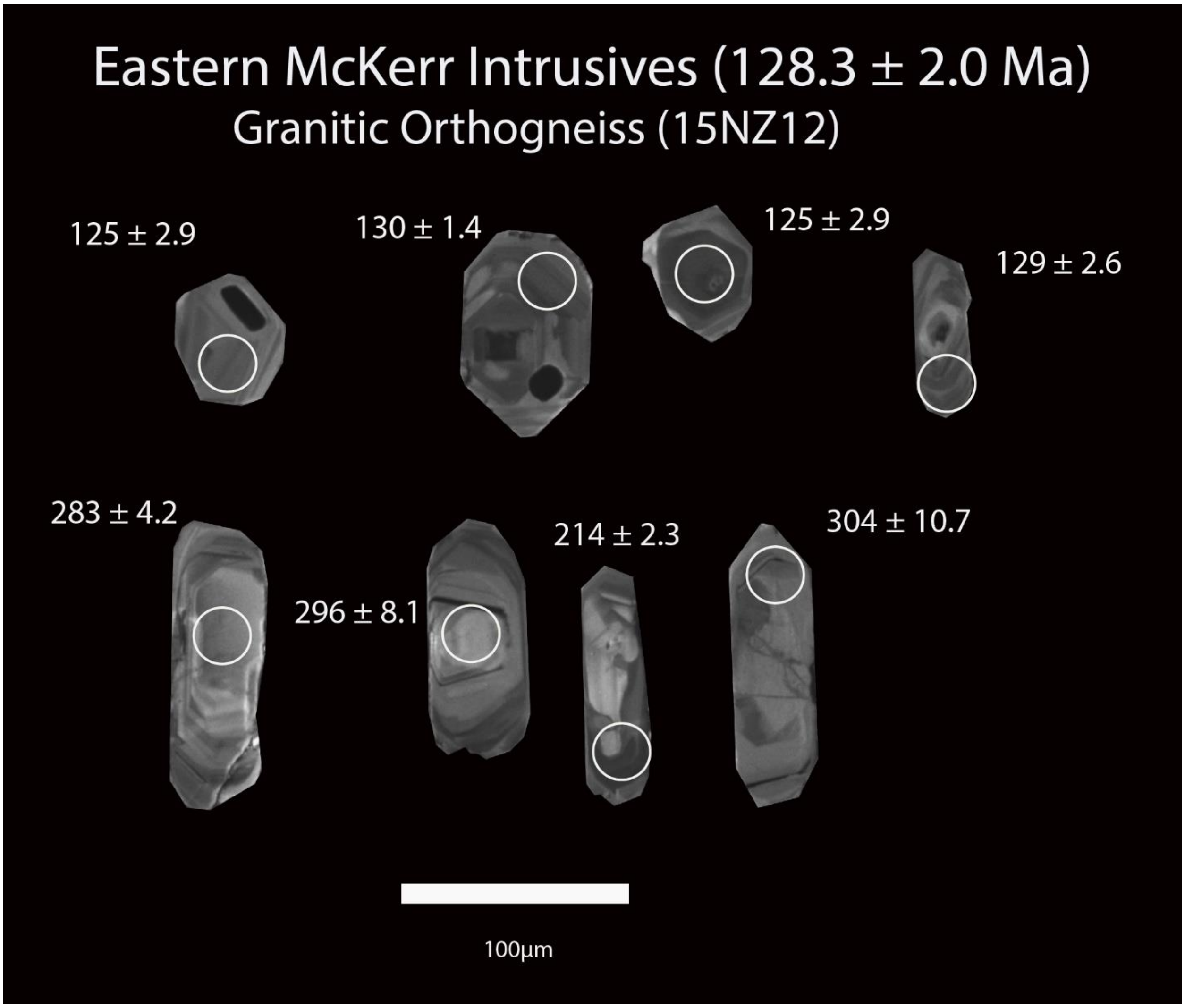
Eastern McKerr Intrusives (128.3 ± 2.0 Ma)
Granitic Orthogneiss (15NZ12)
125 ± 2.9
130 ± 1.4
125 ± 2.9
129 ± 2.6
283 ± 4.2
296 ± 8.1
214 ± 2.3
304 ± 10.7
100µm

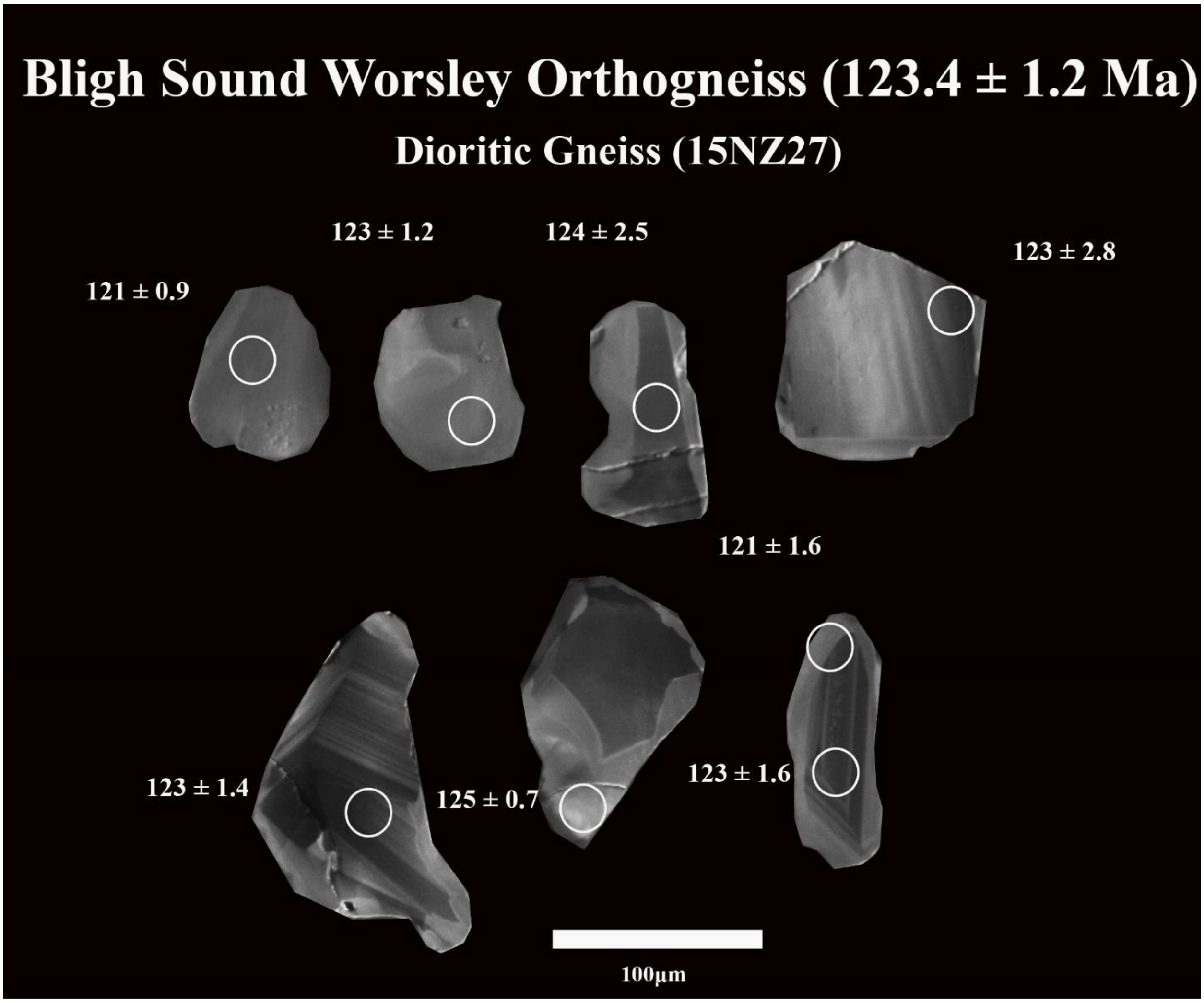
Bligh Sound Worsley Orthogneiss (123.4 ± 1.2 Ma)
Dioritic Gneiss (15NZ27)
123 ± 1.2
124 ± 2.5
123 ± 2.8
121 ± 0.9
121 ± 1.6
123 ± 1.4
125 ± 0.7
123 ± 1.6
100µm